Accepted 27 July 2020

Master Paris Law for Thermal Fatigue of Laminated Composites

Journal of Composite Materials
52(30):1–18

DOI: 10.1177/0021998318776721
www.sagepub.com/

Ever J. Barbero and Javier Cabrera-Barbero

Abstract

A methodology to predict thermal-fatigue damage in laminated composites is presented. Limited data is used to characterize the material system. It is reported that a small number of parameters are enough to characterize the fracture-controlled transverse cracking phenomena and the stress-driven fatigue damage due to defect nucleation and related phenomena. A fatigue damage-initiation criterion and a kinetic equation for fatigue-damage growth are proposed. Further, it is found that Paris Law applies for constant thermal ratio, and that it can be further generalized into a Master Paris Law applicable to arbitrary thermal ratio. These findings form the basis for a methodology to extrapolate available data.

Introduction

A broad variety of composite structures are subjected to thermal fatigue, leading to delaminations, fiber-matrix debonding, loss of hermeticity, and fibers exposure to corrosive environments. Aircraft sit on the tarmac at +60^{o}C and fly at -60^{o}C. With a typical flight schedule of four takeoff and landings/day, they accumulate 1,460 cycles/yr. Low Earth Orbit satellites operating between -156 and 123^{o}C with 90 min orbits, accumulate 5,760 cycles/yr. Windmill blades can be subjected to daily temperature variations up to 57^{o}C plus highly variable wind loads. On the other hand, available thermal fatigue data are limited to only 500 cycles with a few exceptions up to 4000 cycles. Data is scarce because thermal fatigue tests are slow (4–5 cycles/hr); thus, they are performed for few cycles, at few values of thermal ratio, for few laminate stacking sequences. To aggravate matters, the materials properties are temperature dependent[1], thus requiring additional testing effort. Intralaminar transverse cracking in one or more laminas is quantified by the lamina crack density [cracks/mm], which is measurable by various techniques[2] and becomes the state variable for the simulation. Therefore, a methodology is needed to help us design a short yet meaningful testing program, and to extrapolate the data to other situations with confidence.

Experimental observations[3–8] for both quasi-static and mechanical-fatigue loading reveal what crack density rate ($d\lambda/dN$) is fast at the onset of intralaminar damage and tapers off to nearly zero at some point in life N, at a value of crack density λ that is called characteristic damage state

(CDS). Similar behavior is observed at stress raisers such as in OHT and OHC quasi-static tests.[9–12] At CDS, crack density stops growing either because of relaxation of the stress concentration or by the relaxation induced by the onset of delaminations.[13,14]

Crack density evolution studies of *mechanical* fatigue of laminated composites[15–19] point out that CDS seems to be a function of laminate stacking sequence (LSS) and material properties, but apparently independent of loading conditions. Also, experimental data showing similar values of CDS for both, quasi-static and mechanical fatigue up to 4000 cycles is presented in[14]. However, very few studies reach 4000 cycles of *thermal* fatigue due to the difficulty of achieving high number of thermal cycles in a reasonable time, and for those that reach that number, the data does not seem to support reaching CDS at that early number of cycles.[9,10,20–22]

Ample experimental evidence shows that thermal fatigue, as well as mechanical fatigue, reveals itself in the form of transverse cracks, and only at later stages in the "life" of the specimen, other modes of failure such as fiber failure and delaminations may appear. This work investigates *thermal* fatigue using data available in the literature and attempts to develop a simulation based on intralaminar matrix cracking phenomena. Since delaminations are not included in the proposed formulation, applicability of the predictions maybe limited by onset of delaminations at late stages when the number of cycles is sufficiently large.

The temperature ranges used in this manuscript are not related to specific applications but to the availability of experimental data. Viscous effects have not been taken into consideration.

The present formulation is a constitutive model that has been incorporated as a user subroutine in Abaqus®. The constitutive model calculates the damage and reduced stiffness for any temperature and number of cycles. The host Finite Element software (Abaqus in this case) calculates the stress and strain at every Gauss point to maintain equilibrium with the external loads and boundary conditions. The effect of structural boundary conditions are incorporated through the stress/strain field calculated iteratively by the Finite Element software.

The Quasi-Static Problem

In this section we explain how quasi-static fracture mechanics, codified into the Discrete Damage Mechanics Software (Ch. 8 in[23], Ch. 9 in[24]), is used to obtain values for the temperature-dependent fracture toughness* G_{IC} in terms of available experimental data of crack density vs. temperature under quasi-static (no fatigue) conditions.

The bibliography on distributed damage in composite laminates is extensive.[25,26] Among the multitude of damage models available, discrete damage mechanics (DDM) is attractive for this study because, in addition to the usual elastic properties, it requires at most two values of fracture toughness G_{Ic} and G_{IIc} (usually just one needed) to predict both damage initiation and evolution due to transverse and in-plane shear stresses for general laminates subjected to general loads.[27] Since for most materials $G_{IC} < G_{IIC}$, and for most laminates loaded under usual conditions the Energy Release Rates (ERR) are such that $G_I > G_{II}$, only G_{IC} is usually necessary. This is even more true for thermal loading, as show in Fig. 1.

DDM is an objective (mesh independent) constitutive model, meaning that when implemented in FEM software, it does not require guessing of characteristic length L_c in order to reduce mesh

*Although G_{IC} is a critical energy release rate, with units [kJ/m^2], the abbreviated term "fracture toughness" is often used in the composites literature, not to be confused with the classical fracture toughness K_{IC} used for isotropic materials.

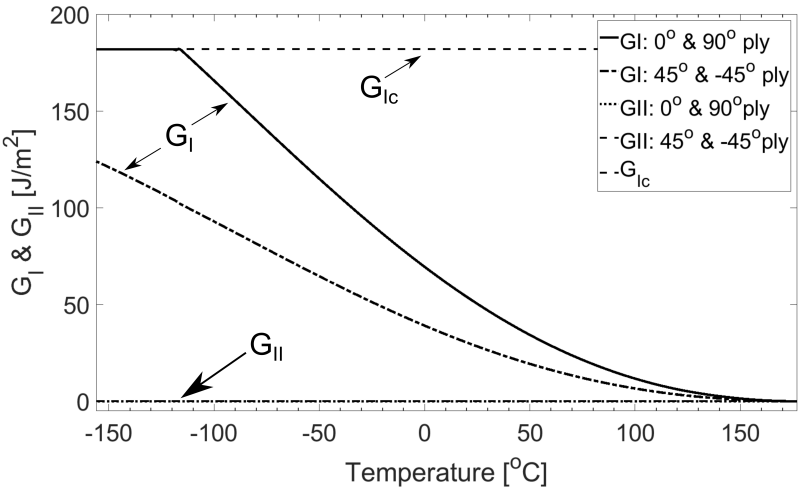

Figure 1. ERR G_I and G_{II} vs. temperature during one thermal cycle for P75/1962 $[0/\pm 45/90]_S$ in the range [-156, 121^{o}C], with stress free temperature SFT=177^{o}C.[1]

dependency.[28] DDM is available as a plugin for Abaqus[24] and ANSYS[29], and it has been extensively validated.

DDM is based on an analytical solution[30] of the displacement field inside a representative volume element (RVE, Fig. 2) encompassing the laminate thickness t with N laminas, a unit length along the fiber direction x_1 of the cracking lamina $k = c$, and a distance $2\ell = 1/\lambda_c$ in the transverse direction x_2. Homogenization of the damaged stiffness of the N laminas, coupled with an iterative procedure allows all laminas $k = 1 \dots N$ in a laminate to be cracking simultaneously with different crack density λ_k values at a given time. For a given damage state $\lambda = \{\lambda_k\}^T$ and applied 2D thermomechanical field $\epsilon = \{\epsilon_1, \epsilon_2, \gamma_6, \Delta T\}^T$ at a Gauss integration point of a shell element, DDM determines the local 3D displacement field $u_i(x_j)$ analytically, with $i, j = 1 \dots 3$, from which it calculates the local strain field and stress field including intralaminar stresses, as well as damaged lamina $[Q]$, damaged laminate stiffness matrices, and energy release rates (ERR) in modes I and II, G_I, G_{II}. The later are used in an interacting damage initiation and evolution criterion

$$g = (1-r)\sqrt{\frac{G_I(\lambda,\epsilon,\Delta T)}{G_{Ic}}} + r\frac{G_I(\lambda,\epsilon,\Delta T)}{G_{Ic}} + \frac{G_{II}(\lambda,\epsilon,\Delta T)}{G_{IIc}} - 1 \leq 0 \tag{1}$$

with $r = G_{IC}/G_{IIC}$. Note that the fracture toughness G_{IC} and G_{IIC} are the only material properties needed to predict both initiation and evolution of crack density under quasi-static conditions, and usually only G_{IC} is necessary. Fatigue loading requires at most two additional parameters, which are the defect nucleation rates β_I, β_{II}, as explained later in this paper. No hardening exponents or any other damage evolution material properties are needed to describe the kinetic evolution of damage. The ERR values G_I, G_{II} in modes $i = I, II$ are calculated as

$$G_i = \frac{U_{i,a} - U_{i,b}}{\Delta A_c} \tag{2}$$

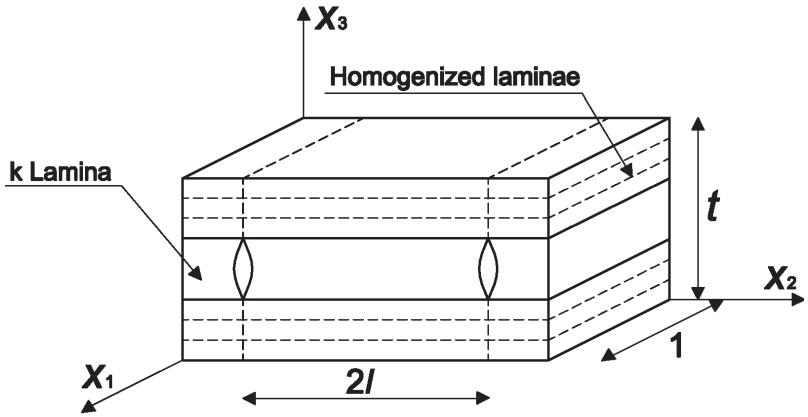

Figure 2. Representative volume element for Discrete Damage Mechanics (DDM).

where $U_{I,a}, U_{I,b}, U_{II,a}, U_{II,b}$ are the elastic strain energies in modes I and II, for crack densities λ_a and $\lambda_b = 2\lambda_a$, and ΔA is the increment of crack area when a new crack propagates (Sect. 8.4.7 in[23]). Mode decomposition is achieved by splitting the strain energy U into mode I (opening) and II (shear) and adding the contribution of each lamina $k = 1 \dots n$ as follows

$$U_I = \frac{V_{RVE}}{2h} \sum_{k=1}^{n} t_k (\epsilon_2 - \widetilde{\alpha}_2^{(k)} \Delta T)\, Q_{2j}^{(k)} (\epsilon_j - \widetilde{\alpha}_j^{(k)} \Delta T) \tag{3}$$

$$U_{II} = \frac{V_{RVE}}{2h} \sum_{k=1}^{n} t_k (\epsilon_6 - \widetilde{\alpha}_6^{(k)} \Delta T) Q_{6j}^{(k)} (\epsilon_j - \widetilde{\alpha}_j^{(k)} \Delta T) \tag{4}$$

where $h = \sum_{k=1}^{n} t_k$, $\epsilon_6 = \gamma_{12}$, and $\widetilde{\alpha}^{(k)}$ are the undamaged CTE of lamina k. Equation (3) is cast in the coordinate system of the cracking lamina k so that ϵ_2 is mode I (crack opening) and ϵ_6 is mode II (crack shear). Laminate ultimate failure is predicted by a fiber damage and failure criterion.[31]

DDM assumes local uniformity of crack spacing and linear distribution of intralaminar stresses in each lamina. Despite these assumptions, predicted results correlate extremely well with available data for a broad variety of material systems (Carbon and Glass reinforced composites), laminate stacking sequences (LSS)[32], and loading conditions including open hole tension data up to failure.[12,31,33,34]

Since the size of the RVE ($1 \times t \times 1/\lambda_k$) is dictated by the crack density λ_k, not by the element size, and the solution is in terms of displacements, not stress or strain, the predictions of the DDM constitutive model are mesh-density and element-type independent. The only effect of mesh density is on the quality of the stress/strain field, as it is well known for the finite element method. Mesh/element-type insensitivity (i.e., model objectivity) is a remarkable advantage with respect to cohesive zone constitutive models that produce results that are mesh-density and element-type dependent.

Thermal fatigue produces intralaminar matrix cracking, resulting in stiffness reduction, stress redistribution that may induce fiber failure, delaminations, and loss of hermeticity. For each fatigue

cycle, intralaminar matrix cracking can be predicted with DDM, which provides a solution for crack density λ [1/mm] in lamina k that can be summarized as follows

$$\lambda = \lambda(G_I, G_{IC}) \quad ; \quad G_I = G_I(\epsilon, \Delta T, Q) \quad ; \quad Q = Q(\lambda) \tag{5}$$

where the function $\lambda()$ calculates the crack density as a function of energy release rate (ERR) G_I and fracture toughness G_{IC}; the function $G_I()$ calculates the ERR as a function mechanical strain ϵ (if applied), temperature range $\Delta T = T_{min} - T_{max}$, and laminate stiffness Q; and finally the function $Q()$ calculates the laminate stiffness as a function of crack density.

Although DDM can be summarized by (5), it is implemented in software, and thus it can also calculate G_I *implicitly* as a function of λ, for a given set of $G_{IC}, \Delta T, \epsilon$, which is useful for the formulation of the fatigue model explained later in this paper. In other words, we can think of the DDM code as capable of solving (5) implicitly for any single variable in (5).

In DDM, an embedded iterative process finds λ for all laminae $k = 1 \dots N$, as a function of applied strain and temperature. It solves for λ inside a representative volume element (RVE) with volume $V = 2LH$, where $2L = L/\lambda$, and H is the laminate thickness.[23] The quasi-static version of DDM is available as a plugin for Abaqus[24] and ANSYS[29], and it has been extensively validated. A plugin for the thermal fatigue version of Discrete Damage Mechanics (DDM6TM) is available in `http://barbero.cadec-online.com/feacm-abaqus/sourceCode.html`.

DDM requires only one material property, the fracture toughness G_{IC} to predict initiation, accumulation, and saturation crack density in a laminate subjected to quasi-static thermal and/or mechanical loading. Thermal stress and temperature-dependent material properties are incorporated. *Fatigue effects are added in this work.*

Matrix cracking of laminates under thermal stress is controlled by the in-situ fracture toughness G_{IC} of the material system. G_{IC} data can be obtained indirectly in terms of the effects of matrix cracking, such as modulus reduction or crack density. Due to the high stiffness of carbon fibers, modulus reduction due to matrix cracks is small and difficult to measure because the modulus reduction in the direction normal to cracks is obscured by the high modulus of non-cracking laminae. Therefore, in this work we use crack density data, which is always measurable by optical, tomography, or acoustic emissions methods, allowing us to simply count the cracks as a function of applied mechanical or thermal strain.[2]

The quasi-static fracture toughness G_{IC} is adjusted from crack density data *at each temperature* by minimizing the error D

$$D = \frac{1}{N}\sqrt{\sum_{j=1}^{N}(\lambda_j - \lambda_j^d)^2} \tag{6}$$

between crack density λ_j predicted with (5) and experimental λ_j^d crack density data *at each temperature*. The temperature-dependent results are then fitted as a function of temperature with a quadratic polynomial

$$G_{IC} = a + bT + cT^2 \tag{7}$$

with parameters a, b, c shown in Table 1. A temperature-independent (average) value of G_{IC} can be obtained by using all the data for all temperatures at once in (6), with values shown on the next to last column of Table 1. The results are plotted in Fig. 3, where it can be seen that the temperature-dependence of G_{IC} is not strong. This is due to the compensating effects of the material becoming more brittle but with a lower CTE at low temperature.[1]

Table 1. Temperature dependent fracture toughness for Carbon/Epoxy P75/1962 adjusted from crack density data vs. temperature.

Material	V_f	Temperature range [^{o}C]	a	b	c	G_{IC}	Ref.
P75/934	0.65	[-160,20]	50.0561	-4.3006 10^{-2}	6.3749 10^{-4}	53.4050	[35]
P75/1962	0.52	[-160,-15]	77.8054	9.6211 10^{-2}	1.3948 10^{-3}	84.4808	[10]
AS4/3501-6	0.64	[-190,20]	61.9052	-1.6097 10^{-1}	-5.0412 10^{-4}	68.0664	[9]

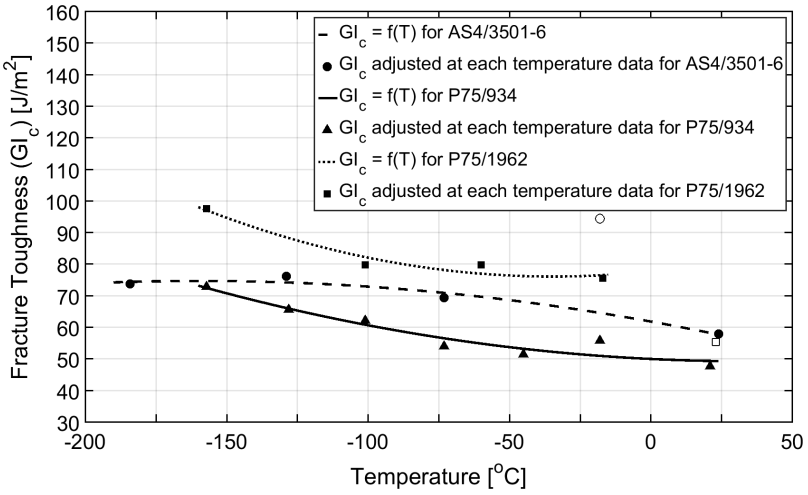

Figure 3. G_{Ic} vs. temperature for P75/934, P75/1962, and AS4/3501-6.

The First Cycle of a Fatigue Test

This section provides background for the fatigue phenomenon presented in the following section. We introduce the concept of crack propagation being initiated at large enough defects such as voids and crazes. Such propagation is governed by energy considerations rather than stress.

The Griffith/Irwin *fracture criterion* is used in this work as *damage-initiation criterion*, taking into account that a single intralaminar matrix crack does not by itself causes *fracture* of the whole laminate, but rather contributes to the deterioration of the laminate in the form of *damage*. The Griffith/Irwin *fracture criterion* states that when the Energy Release Rate (ERR) G_I exceeds the fracture toughness G_{IC}, a new crack appears, i.e.,

$$\xi = \frac{G_I}{G_{IC}} \geq 1 \rightarrow \text{new intralaminar crack} \tag{8}$$

According to Irwin, inelastic dissipation at the crack tip is included in G_{IC}, because the polymer is quasi-brittle and the plastic zone is small with respect to the crack dimensions, which is satisfied for this problem because the crack size is equal to the lamina thickness, and thus much larger than the plastic zone.[30] Therefore, quasi-static DDM[23,24,29] can be used to calculate crack density as a function of applied strain and/or temperature, or alternatively ERR as a function of crack density for fixed strain and temperature. The stress intensity K_I and ERR can be written (Ch. 6 in[36]) as $K_I = \beta\sigma\sqrt{\pi t_k}$ or

$$G_I(\lambda) = \beta^2 t_k (1-\nu^2) E(\lambda) \epsilon^2 \tag{9}$$

where t_k is the thickness of lamina k, ϵ is the applied thermo-mechanical strain, and β is a geometric coefficient that accounts for the geometry of the crack and the domain. DDM calculates the degraded material properties $\nu(\lambda), E(\lambda)$ and the geometric coefficient β. The strain is $\alpha\Delta T$. Therefore the fracture problem is solved if we know the fracture toughness G_{IC}.

For the first cycle (N=1) of a thermal fatigue test, we use the classical fracture toughness G_{IC} of the material (Table 1). Note that crack density is driven by energy considerations, specifically by energy release rate. If sufficient energy is available to propagate a crack, the Griffith/Irwin criterion states that the crack will actually propagate. It has nothing to do with stress. Furthermore, the energy required for crack formation (twice Griffith's surface energy plus Irwin's crack-tip dissipation effects) comes from the entire laminate, no just from the lamina that is cracking. This energy becomes available due to the relaxation caused by the propagation of the crack itself. This is in contrast to the fatigue problem, which is driven by stress, as we shall see in the next section. Also, there are no long-range dissipation effects such as fiber bridging because intralaminar cracks propagate mostly in the matrix.

For N=1, cracks propagate at all locations where initial defects are large enough. Once those defects propagate into cracks, no more defects remain that are large enough to propagate into cracks, unless the mechanical or thermal strain are increased, or some other physical phenomenon, such as fatigue, produces new large enough defects that can grow into cracks, as explained in next section. Note that under constant amplitude mechanical or thermal fatigue, the applied strain (mechanical or thermal) remains constant. All the defects that are large enough to grow into cracks are used during the first cycle, and on the next cycles there are no sites that can propagate into cracks, unless fatigue manages to nucleate small defects into large enough defects that can act as viable sites for crack propagation.

When crack density increases, the stiffness $E(\lambda)$ and coefficient of thermal expansion (CTE) $\alpha(\lambda)$ decrease.[1] The strain $\epsilon = \alpha\Delta T$ decreases because the CTE decreases while ΔT is constant, and the ERR G_I decreases as per (9) with both E and ϵ decreasing. Once the ERR and strain decreases, no more cracks can appear unless either the strain increases or the fracture toughness decreases. The strain cannot increase because the temperature range is constant, and the fracture toughness is an invariant material property (Table 1). For fatigue damage to occur when $N > 1$, the *fatigue fracture toughness* must decrease, as discussed next.

Fatigue Damage Criterion

In this section we propose a *fatigue damage criterion* using separation of variables to describe fatigue-damage as the product of an energy-controlled fracture problem times an stress-controlled void and defect nucleation problem.

Thermal fatigue is caused by cyclic, repetitive oscillation of temperature T in the range $T_{min} < T < T_{max}$, with amplitude $\Delta T = T_{min} - T_{max} < 0$, thermal strain $\epsilon = \alpha\Delta T$ and thermal ratio defined as $R = T_{min}/T_{max}$.

Since the *quasi-static* fracture toughness G_{IC} is an invariant material property, the fatigue effect must be represented separately. In this work we propose to use separation of variables to write the *fatigue* fracture toughness G'_{IC} as the product of the quasi-static fracture toughness G_{IC} times the proposed defect nucleation function $f(N)$, as follows

$$G'_{IC} = G_{IC} \cdot f(N) \quad ; \quad 0 < f(N) < 1 \tag{10}$$

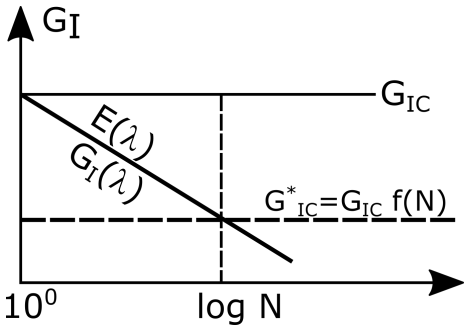

Figure 4. As λ grows, $E(\lambda)$ decreases, $G_I(\lambda)$ decreases, and no new cracks can be propagated unless $f(N)$ decreases, which requires $N > 1$, thus fatigue loading.

Then, generalizing (5) for fatigue

$$\lambda = \lambda(G_I, G'_{IC}) \quad ; \quad G_I = G_I(\epsilon, \Delta T, Q) \quad ; \quad Q = Q(\lambda) \tag{11}$$

we can calculate crack density for every cycle with $N > 1$.

To explain the sequence of events during thermal fatigue loading, let's look at Fig. 4. For $N = 1$, the material is pristine, thus $f(N) = 0$, and the Griffith/Irwin condition (8) means that ΔT must be large enough to produce enough thermal strain to propagate a crack from the largest existing defect in the material. If ΔT is not large enough, more cycles $N > 1$ are needed to grow the existing defects, for example by void/craze nucleation, so that a critical size is reached and the first crack can be propagated.

Once a crack is propagated, λ grows, $E(\lambda)$ decreases, and $G_I(\lambda)$ decreases. Since G_{IC} is constant, no new cracks can be propagated unless $f(N)$ decreases, which requires $N > 1$, thus fatigue loading.

With G_{IC} constant, as $f(N)$ reduces due to defect nucleation, fatigue toughness $G'_{IC} = G_{IC}\ f(N)$ can decrease sufficiently to catch up with decreasing ERR $G_I(\lambda)$ and thus, fatigue can take place.

The physical justification is as follows. In the absence of new cracks, cyclic load (mechanical or thermal) results in nucleation of voids and crazes in the polymer. Crazes are broken polymer branches and chains that occur due to stress.[37,38] They multiply and coalesce into larger defects, driven by hydro-static stress.[37,38] When the void or craze is large enough, a crack can propagate.

Thus, fatigue is a stress-driven phenomenon, not an energy-driven phenomenon. This provides justification for separating the fatigue phenomenon into an energy-driven quasi-static fracture toughness G_{IC} and a stress-driven defect nucleation function $f(N)$.

The defect nucleation function $f(N)$ can be characterized using low-cycle experimental data as follows. Crack density vs. number of cycles can be obtained from experimental data (shown by symbols in Fig. 5). For those cracks to be present, the Griffith/Irwin criterion demands that $G_I = G'_{IC}$. DDM can calculate G_I given λ and ΔT. Therefore, using Eq. (11), DDM calculates the fatigue ERR G_I that corresponds to any set of known crack density λ, temperature range ΔT, and life N. Using the fracture criterion $G_I = G'_{IC}$, we immediately know what the value of G'_{IC} is. Then, discrete values for the defect nucleation function $f(N)$ can be obtained from (10) by dividing G'_{IC} by the constant G_{IC} (from Table 1). The resulting discrete values of $f(N)$ are displayed by square symbols Fig. 6.

The relationship between $f(N)$ and $\log(N)$ seen in Fig. 6 can be approximated by

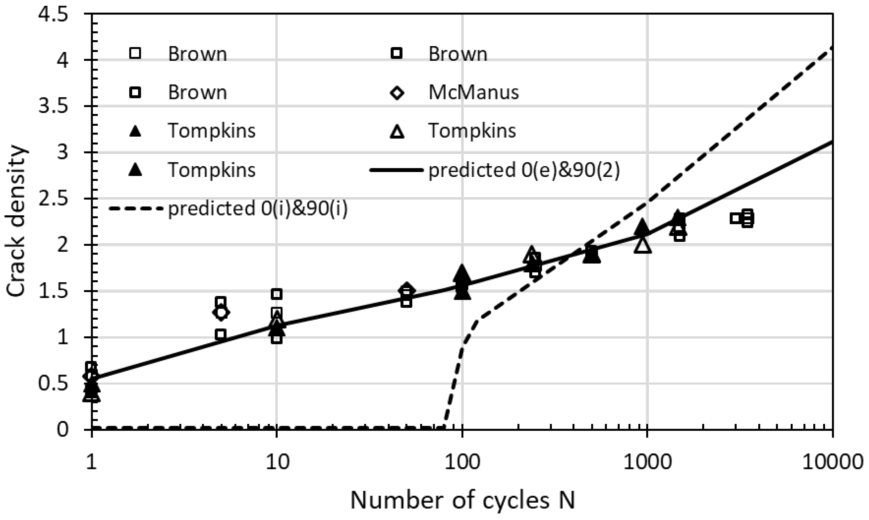

Figure 5. Experimental crack density vs. number of cycles (N=1...3500) with thermal ratio $R = -156/121\ ^{o}$C, for Carbon/Epoxy P75/1962 $[(0/90)_2]_S$, data from[10,21,22].

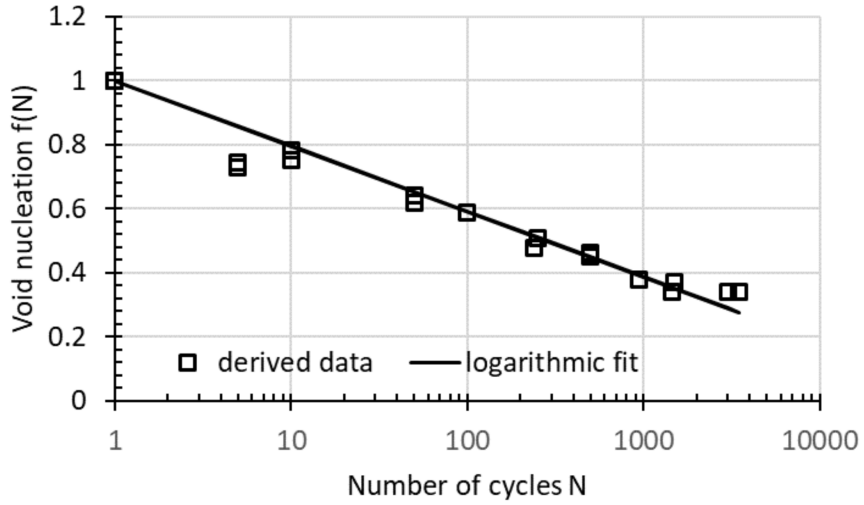

Figure 6. Characterization of the defect nucleation function f(N) using experimental data from Fig. 5. The linear fit has a slope $\beta = 2.04$.

$$f(N) = 1 - \beta \log N \tag{12}$$

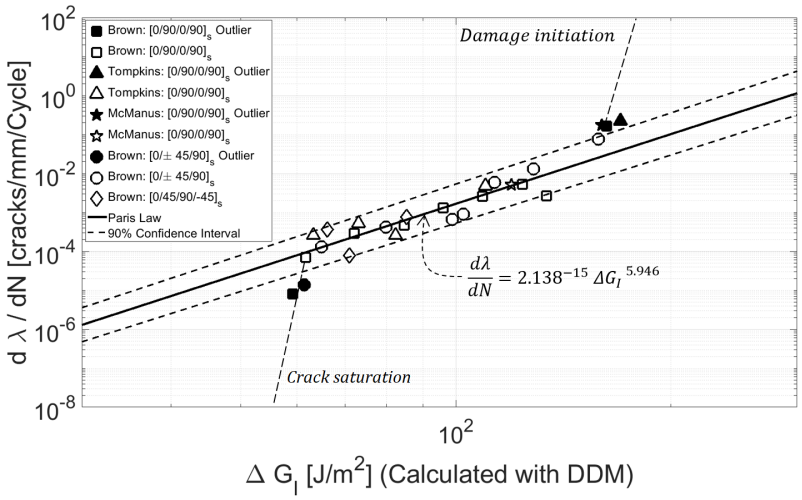

Figure 7. Paris Law. All data has the same thermal ratio $R = -156/121$ °C and $T_{min} = -156^o$C.

with $\beta > 0$. The defect nucleation function $f(N)$ is decreasing with N, so that with constant quasi-static fracture toughness G_{IC}, the fatigue fracture toughness G'_{IC} in (10) becomes a decreasing function of N, thus allowing for the fatigue phenomenon to be represented.

Master Paris Law

In this section we propose a *kinetic equation for fatigue-damage growth* extending the modified Paris Law[39†] to define the Master Paris Law. This exercise provides further insight into the kinetics of fatigue damage in laminated composites, leading to a procedure that not only describes the data but also allows us to propose and extrapolation method for laminate stacking sequences (LSS), thermal ratio R, and life N beyond the limitations of the experimental data. While only experimental data may someday prove or disprove the proposed method, numerical results agree with experimental data that is available only for a modest range of number of cycles.

Using experimental data $\lambda(N)$, such as that available in Fig. 5, we calculate the crack-growth rate $d\lambda/dN$ as the slope of the data. Then, use (11) to calculate $\Delta G_I = G_I(T_{min}) - G_I(T_{max})$ for each value of $d\lambda/dN$, and finally plot $d\lambda/dN$ vs. ΔG_I as in Fig. 7.

The resulting data in Fig. 7 can be approximated accurately by a linear equation, which is known as modified Paris Law:

$$\frac{d\lambda}{dN} = a\ [\Delta G_I(\lambda, \Delta T)]^b \tag{13}$$

with parameters a, b.

The outlier data (dark symbols) deviate from the modified Paris Law, thus suggesting particular events that can be attributed to damage initiation and crack saturation. Damage initiation is evident

† *Modified* means that crack density and energy release rate substitute crack length and stress intensity K_I in the original Paris Law.

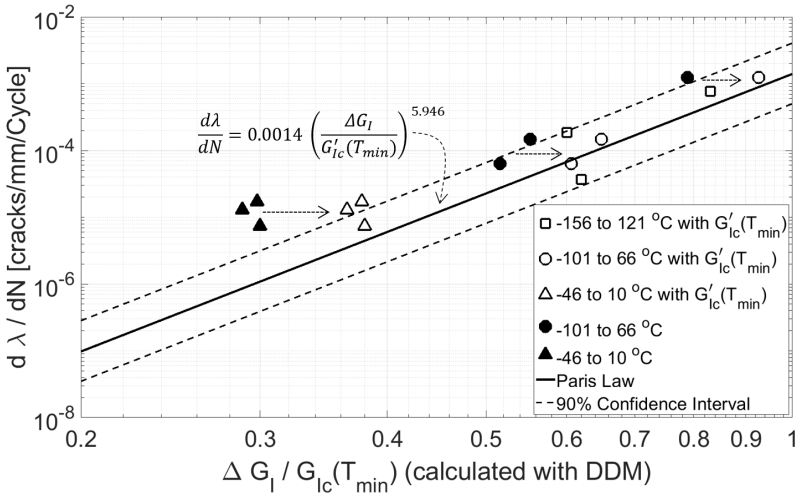

Figure 8. Master Paris Law for multiple thermal ratios $R = -156/121, -101/66$, and $-46/10^{o}$C, all shifted with their value of T_{min}

at the top-right of Fig. 7, where both ΔG_I and $d\lambda/dN$ are large. Crack saturation is evident at the bottom-left of Fig. 7, where ΔG_I and $d\lambda/dN$ are small.

On Fig. 7, the thermal ratio R is the same for all data. But data with different thermal ratio does not fit the modified Paris Law, as shown by the dark symbols in Fig. 8. To solve this problem, we note that a constant slope in log scale suggest Arrhenius phenomena. Therefore, taking a clue from the time-temperature superposition principle, [40] we propose to normalize (shift) ΔG_I by $G_{IC}(T_{min})$, as shown in Fig. 8, which can be described by the proposed Master Paris Law equation:

$$\frac{d\lambda}{dN} = A \left[\frac{\Delta G_I(\lambda, \Delta T)}{G_{IC}(T_{min})}\right]^b \tag{14}$$

with recalculated parameter A. For a given data set, parameter b is unaffected by the shift. Thus, equation (14) is proposed here as a kinetic equation for damage growth-rate during thermal fatigue of laminated composites.

Note that in log scale, a quotient is a shift. The quasi-static fracture toughness at the lowest temperature $G_{IC}(T_{min})$ is chosen as the shift factor because maximum crack propagation takes place at temperature T_{min}, where the thermal stress is maximum and the polymer is most brittle. After the shift, all data fits in the 90% confidence interval regardless of thermal ratio.

Master Paris Law (MPL) works as the temperature-time superposition principle (TTSP). We can find the parameters a and b by testing with low thermal ratio, such as $R = -46/10$ and $R = -101/66$, which is are easy tests, then shift the data (dark symbols in Fig. 8) to $T_{min} = -156$ and have a Paris Law for any situation with $T_{min} = -156^{o}$C.

Comparison of predicted crack density vs. number of cycles $\lambda(N)$ with experimental data is presented in Fig. 5, for R=-156/121, for which most thermal fatigue experimental data is available. On the other hand, Fig. 7 shows how the data for thermal ratio R=-156/121 can be represented by Paris Law. Note that for data at a single thermal ratio, there is no need to invoke the *Master* Paris Law, but just Paris Law is enough. However, once multiple thermal ratios are considered, Paris

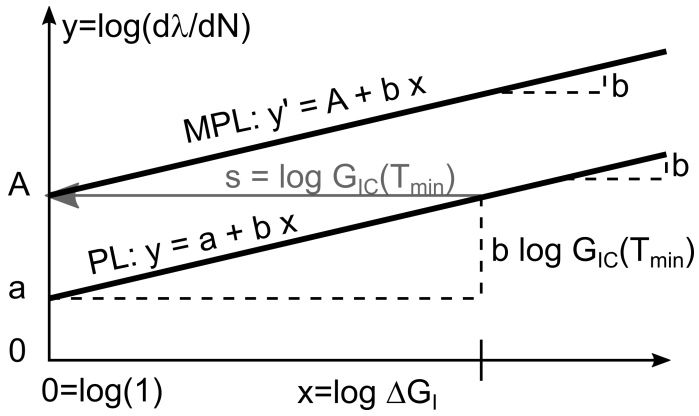

Figure 9. Determination of constant A in Master Paris Law.

Law is not enough. Fig. 8 shows how the shifted data for all thermal ratios (namely R=-156/121, -101/66 and -46/10) aligns itself along the *Master* Paris Law line. Once the shifting procedure is proven, the *Master* Paris Law line can be shifted to any temperature. That is, the *Master* Paris Law line can be shifted and then used for analysis at any temperature.

Since the shift temperature T_{min} is our choice, we can actually have a Paris Law for any temperature. Further, note that T_{max} does not participate in the shifting process, but instead is taken into account by DDM during calculation of ΔG_I.

Since ΔG_I is a function of life N and temperature range T_{min}, T_{max}, we can calculate damage rate $d\lambda/dN$ for any set of values N, T_{min}, T_{max}, regardless of what temperature range was used to obtain the material properties a, b. Since a is a function of the shift temperature T_{min} and the slope b is a constant, independent of shift temperature, we can derive a formula for the constant A in MPL. With reference to Fig. 9 we have

$$A = a + b \cdot s \quad \text{with shift } s = \log G_{IC}(T_{min}) \tag{15}$$

The only constraints on the applicability of shifting are Damage Initiation (DI) and Crack Saturation (CS), as illustrated in 7, where the applicable region is bracketed by DI on the top-right and CS on the bottom-left. The proposed formulation accounts for this bracketing implicitly. Nothing special has to be coded in the software to account for it.

For a situation characterized by N, T_{min}, T_{max}, all of which are independent variables for the analysis, DDM will correctly calculate damage initiation, so that the portion of the MPL on the right of "damage initiation" is unused (see Fig. 8). If damage initiation were not to occur at $N = 1$, the software tries for higher N until $f(N)$ decreases enough to allow the first crack to propagate. In either case, the portion of the MPL on the right of "damage initiation" is unused.

Similarly, for sufficiently large values of N, DDM predicts that $\Delta G_I \to 0$, because $E(\lambda) \to 0$, so the left portion of the MPL will not be used (see Fig. 8). This can be seen in Fig. 10 at $n = 10^5$, where it is evident that after crack density reaches a maximum, the material is damaged so much that the ERR G_I that would be released as a result of another crack is insufficient to exceed the fatigue fracture toughness $G'_{IC} = G_{IC} f(N)$ even though G'_{IC} is decreasing because $f(N)$ is decreasing with increasing N. In Fig. 8, at $N = 10^5$ the predicted crack density drops, but in reality damage is irreversible, so the software detects it and keeps the crack density constant at the maximum value.

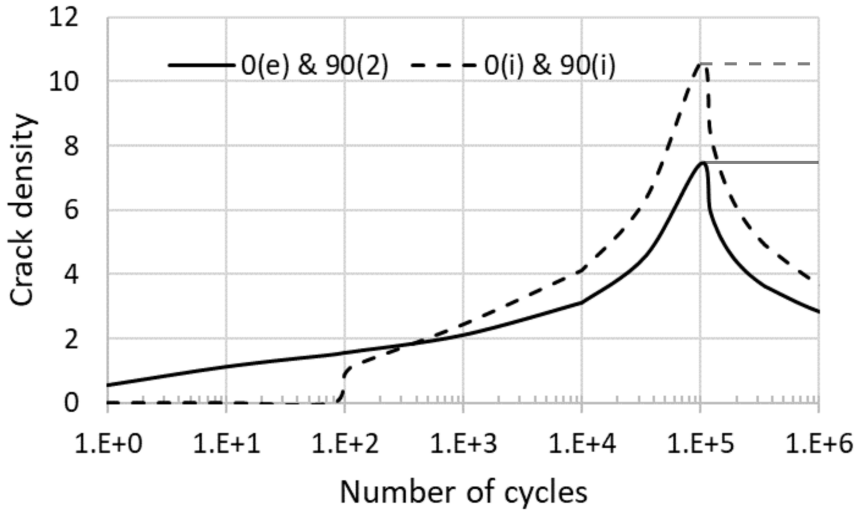

Figure 10. Predicted crack saturation at $N \approx 10^5$.

Thermal and Fatigue Damage Prediction

The current implementation of DDM, called DDM6TM (version 6, thermomechanical) can analyze two situations, as follows:

Monotonic Cooling simulates cooling of the material from Stress Free Temperature (SFT) down to the coldest analysis temperature (T_{min}) for cycle one (N=1); that is, no fatigue phenomenon is apparent ($f(N) = 1$). The total temperature excursion $\Delta T = T_{min} - SFT$ is divided in 1^oC increments. Crack density is calculated at the end of each increment. The temperature-dependent properties at the beginning of the increment are used. Ply-by-ply stress and strain components, energy release rate (ERR), and crack density are calculated at each temperature.

For example, crack density at T_{min} in the center ply of a $[(0/90)_2]_S$ laminate, clamped all around, is shown in Fig. 11. The fiber direction is vertical for the 90_2 center lamina. When the material cools and shrinks, thermal contraction imposes tensile stress across the fibers that is maximum at the edge of the hole (blue color, left figure), causing maximum damage at the edge of the hole (red color, right figure).

Thermal Fatigue Damage occurs when the temperature is cycled with constant thermal ratio $R = T_{min}/T_{max}$ with $T_{min} < T_{max} \leq SFT$ and $\Delta T = T_{min} - T_{max}$. Since the maximum crack density in each cycle occurs at T_{min}, the crack density is calculated at temperature T_{min}.

The reduction of fatigue toughness G'_{IC} with number of cycles and temperature is accounted for by two parameters, the quasi-static fracture toughness G_{IC} and the defect nucleation function $f(N)$. The temperature-dependent, quasi-static fracture toughness is a material property that can be obtained from quasi-static testing (at $N = 1$) as explained in[1]. The defect nucleation function can inferred from experimental data as explained in this work. For

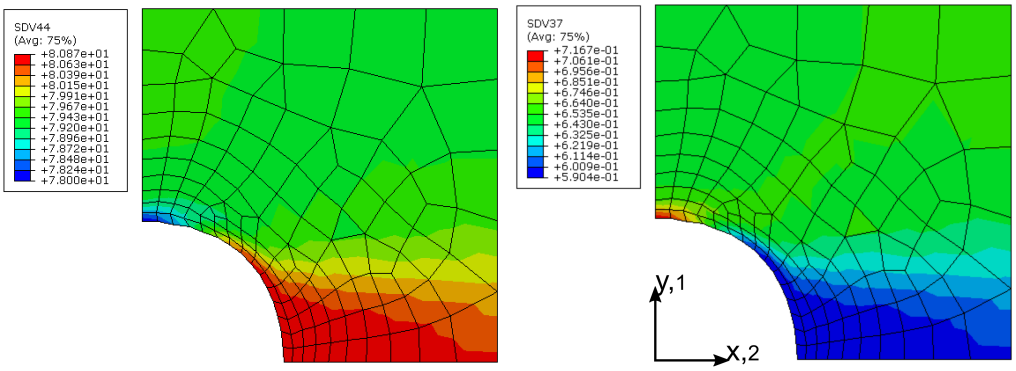

Figure 11. Left: SDV44=σ_{22} at $T_{min} = 57^o$C in the center lamina of a $[(0/90)_2]_S$ laminate clamped all around, SFT=177^{o}C. Right: SVD37=crack density. 1/4 model shown. σ_{22} is smaller where the damage is higher.

every cycle N, the software calculates crack density, ply-by-ply stress and strain distributions, and energy release rate (ERR). Crack density vs. life N is compared to experimental data in Fig. 5 (solid line).

For a laminate with n laminas, the proposed methodology finds the crack density that is compatible with the Griffith/Irwin condition $G_I = G'_{IC}$ with $G'_{IC} = G_{IC}\ f(N)$, G_{IC} constant, and $f(N)$ decreasing with N as shown in Fig. 6.

Comparison of crack density vs. number of cycles predicted with the proposed methodology and experimental data[10,21,22] for $[(0/90)_2]_S$ is shown in Fig. 5. Data is only available for exterior [0] and interior [90_2] laminas. From quasi-static studies, these laminas are known to crack earlier and proceed with slower crack growth rate than thinner, interior laminas (Fig. 7.9 in[23]). Data is not available for the interior [0] and [90] single-ply laminas, but the predicted values for interior laminas (dash line) are consistent with previous experimental and analytical results for laminates are subjected to quasi-static, strain-controlled loading, that show that interior laminas crack later and proceed with faster crack-growth rate. Thus, the fatigue crack-growth rates shown in Fig. 5 are consistent with previous quasi-static data. For the exterior [0] and interior [90_2] laminas, the agreement between prediction and data is good.

Agreement with experimental data is demonstrated in Fig. 5 up to 3500 cycles. Beyond that, there is no experimental data available, but the proposed methodology is able to predict the response as shown in Fig. 10. A crack density peak is predicted at approximately $N = 10^5$ when the *crack saturation (CS)* is reached. Since crack density is so high, ERR is very small, and the only way to satisfy the Griffith/Irwin condition is for the software to unrealistically lower the crack density. Thus, the onset of a negative rate of crack density evolution can be used to detect CS. After that number of cycles, the crack density remains constant, as show by the grey line in Fig. 10. This type of behavior is consistent with experimental observations under mechanical fatigue loads for a different LSS and material system,[14] but thermal loads seem to tolerate higher values of crack density. Note however, that the current formulation does not account for delaminations, which may lower the CS significantly.

Implementation

The independent variables for the analysis are N, T_{min}, T_{max}. The range for N and values for T_{min}, T_{max} are to be provided as input to the software.

The dependent variables are the crack density $\lambda(k)$ in each lamina k, and from that, it is possible to calculate the ERRs $G_I, G_{II,}$ that produced such crack density, as well stress components in each lamina. These variables constitute the output of the software.

The material properties are temperature dependent. The quasi-static fracture toughness G_{IC}, G_{IIC}, are quadratic in temperature, with three coefficients a, b, c, for each property, as in (7). They can be adjusted to crack density data for monotonic cooling (N=1) as described in [1].

The elastic properties $E_1, E_2, G_{12}, \nu_{12}, \nu_{23}$ are quadratic in temperature, with three coefficients a, b, c, for each property, representing the constant, linear, and quadratic terms, respectively. They can be adjusted to available data as described in [1].

Each cycle of a thermal fatigue problem starts at SFT, cooling the material down to T_{max}. Then, further cooling to T_{min} and back up to T_{max}, thus completing one cycle. The analysis must begin at SFT so that residual thermal stresses are accounted for. Therefore, three temperatures must be specified at the onset of the analysis: SFT, T_{max}, T_{min}.

The CTE values α_1, α_2, are cubic in temperature, with four coefficients a, b, c, d, for each property, representing the constant, linear, quadratic, and cubic terms, respectively. They can be adjusted to available data as described in [1].

Fiber failure is monitored using the model in [31], which requires the lamina tensile and compression strength in the fiber direction F_{1T}, F_{2C}, as well as the Weibull modulus of the fiber. [23] The lamina compression strength in the transverse direction F_{2C} is included in the script in anticipation of future work, but that aspect is still not implemented.

Finally, the defect nucleation function for transverse mode I and shear mode II are represented by one coefficient each, β_I, β_{II}, as in (12). Since mode II ERR is small for thermal loads (Fig. 1), it is assumed that the mode II component of ERR does not play a significant role. Therefore, only G_{IC} data is usually needed, but the software implements the mode II as well in case it becomes necessary in the future. The parameters β_I, β_{II}, are not necessary for thermomechanical analysis during the first cycle (N=1) but they are necessary for thermal fatigue predictions. Similarly to G_{IIC}, the defect nucleation rate β_{II} is usually not needed when the laminate is subjected to thermal loads.

The input parameters can be provided to Abaqus using an Abaqus Python script or through the .inp file. An Abaqus script is provided as supplemental material, available on the Journal's website. The provided script includes additional code for tasks that are usually performed with the graphical user interface (CAE), such as mesh generation and specification of boundary conditions, so that all the code to execute and example is available in a single file. The script is set up to perform either monotonic cooling or fatigue calculations.

Fig. 11 is made with Abaqus/CAE using the results saved by the DDM6TM plugin via SDV's. In Abaqus, SDV's are meant to store state variables (e.g., crack densities for all laminas, at each Gauss point), but we also use them to store derived quantities, such as stress and ERR's, to allow for visualization.

For each lamina we save 12 values:

SDV1 Crack density λ_k in lamina k with $k = 1 \ldots n/2$ for a symmetric laminate, with $k = 1$ at the bottom of the laminate.

SDV2 Longitudinal tensile damage activation g_{1t} [31]

SDV3 Longitudinal compression damage activation g_{1c} (not implemented)

SDV4 Longitudinal tensile damage D_{1t}, derived from SDV2[31],[24] (9.32)

SDV5 Transverse damage D_2, derived from SDV1[24] (9.32)

SDV6 Shear damage D_3, derived from SDV1[24] (9.32)

SDV7 Longitudinal stress in lamina c.s.

SDV8 Transverse stress in lamina c.s.

SDV9 Shear stress in lamina c.s.

SDV10 Transverse damage activation function g_{2t}[23] (8.24)

SDV11 Energy Release Rate mode I, $G_I(\lambda)$ (present work,[23] (8.43))

SDV12 Energy Release Rate mode I, $G_I I(\lambda)$ (present work,[23] (8.44))

Upon completion of the Abaqus Job, the SDVs can be used for visualization within Abaqus/CAE.

Conclusions

Separation of variables highlights the multi physics of fatigue degradation, with damage onset controlled by fracture toughness and kinetics controlled by defect nucleation. Besides temperature-dependent material properties (modulus, and CTE), predicting fatigue damage requires characterization of one temperature-dependent fracture toughness (mode I) and the constant defect nucleation rate (beta I). The former can be obtained from a quasi-static cooling test and the later from a low-cycle thermal fatigue test. Both tests involve counting transverse cracks as a function of either temperature or number of cycles. The fatigue data is also used calculate the two coefficients (a,b) in Master Paris Law, which provides the kinetic equation describing crack growth rate. New cracks appear at the lowest temperature, where the material is most brittle and thermal stress maximum. Master Paris Law allows for data extrapolation to various LSS and thermal ratios R=Tmin/Tmax, potentially allowing for extrapolation to number of cycles N larger than the largest number of cycles of the experimental data. Predictions are consistent with observed phenomena.

Supplemental materials

Abaqus script The Abaqus scripts to reproduce the results displayed in this paper, both thermal-only and thermal-fatigue analyses, are available at `http://barbero.cadec-online.com/feacm-abaqus/Examples/Chapter_9/Ex_9.2/`.

Link for downloading the Abaqus plugin A plugin for the thermal fatigue version of Discrete Damage Mechanics (DDM6TM) is available at `http://barbero.cadec-online.com/feacm-abaqus/sourceCode.html`.

Acknowledgments

We thank SIMULIA® for making available to us the SIMULIA Academic Research Suite for the completion of this project, of which we have used Abaqus/Standard and taken advantage of its user programmable features. Abaqus and SIMULIA are registered trademarks of Dassault Systèmes or its affiliates.

References

1. E. J. Barbero and J. Cabrera Barbero. Damage initiation and evolution during monotonic cooling of laminated composites. *J. Composite Materials, 52(30), 4151–4170*, 2018.
2. A. M. Abad Blazquez, M. Herraez Matesanz, C. Navarro Ugena, and E. J. Barbero. Acoustic emission characterization of intralaminar damage in composite laminates. *MATCOMP XIII, Algeciras, Spain*, pages 33–38, 2013.
3. Reifsnider K and Masters J. *Investigation of characteristic damage states in composite laminates.* ASME, 1978.
4. Reifsnider K and Highsmith A. *Materials: experimentation and design in fatigue*, chapter Characteristic damage states: a new approach to representing fatigue damage in composite laminates. 1981.
5. Jamison R, Schulte K, Reifsnider K, and Stinchcomb W. Characterization and analysis of damage mechanisms in tension-tension fatigue of graphite epoxy laminates. *ASTM STP;836:21-55.*, 1984.
6. Takeda N and Ogihara S. Initiation and growth of delamination from the tips of transverse cracks in cfrp cross-ply laminates. *Compos Sci Technol; 52:309-18*, 1994.
7. Zubillaga L, Turon A, Renart J, Costa J, and Linde P. An experimental study on matrix crack induced delamination in composite laminates. *Compos Struct.;127:10-7*, 2015.
8. Carraro P, Novello E, Quaresimin M, and Zappalorto M. Delamination onset in symmetric cross-ply laminates under static loads: theory, numerics and experiments. *Compos Struct. 176, pp. 420-432*, 2017.
9. J. R. Maddocks. Microcracking in composite laminates under thermal and mechanical loading. *NASA Technical Report N96-16101*, 1995.
10. H. L. McManus. Prediction of thermal cycling induced matrix cracking. *Journal of Reinforced Plastics and Composites, 15:124–140*, 1996.
11. C.H. Park and H.L. McManus. Thermally induced damage in composite laminates predictive methodology and experimental investigation. *Compos Science and Technology;56:1209-1219*, 1996.
12. M.M. Moure, S.K. Garcia-Castillo, S. Sanchez-Saez, E. Barbero, and E.J. Barbero. Matrix cracking evolution in open-hole laminates subjected to thermo-mechanical loads. *Composite Structures*, 183(-):510–520, 2018.
13. Johnson P. and Chang F. Characterization of matrix crack-induced laminate failure – part I: experiments. *J Compos Mater;35:2009-35*, 2001.
14. Hamed Pakdel and Bijan Mohammadi. Characteristic damage state of symmetric laminates subject to uniaxial monotonic-fatigue loading. *Engineering Fracture Mechanics 199:86-100*, 2018.
15. Carlsson L., C. Eidefeldt, and T. Mohlin. Matrix cracking induced by cyclic ply stresses in composite laminates. *ASTM STP;907:361-82*, 1986.
16. Lee J, Daniel I, and Yaniv G. Fatigue life prediction of cross-ply composite laminates. *ASTM STP;1012:19-28*, 1989.
17. C Henaff-Gardin, I Goupillaud, M Lafarie-frenot, and S Buhr. *12th international conference on composite materials*, chapter Modelling of transverse cracking under uniaxial fatigue loading in cross-ply composite laminates: experimental validation. Paris, France, 1999.
18. M Lafarie-Frenot, C Henaff-Gardin, and D. Gamby. Matrix cracking induced by cyclic ply stresses in composite laminates. *Compos Sci Technol;61:2327-36*, 2001.
19. J. Llobeta, P. Maimí, Y. Essab, and F. Martin de la Escalera. Progressive matrix cracking in carbon/epoxy cross-ply laminates under static and fatigue loading. *International Journal of Fatigue, 119, 330-337*, 2019.
20. H. L. McManus. Prediction of thermal cycling induced cracking in polymer matrix composites. *NASA Technical Report NAG-1-1493*, 1994.

21. S. S. Tompkins, J. Y. Shen, and A. J. Lavoie. Thermal cycling of thin and thick ply composites. *NASA TR NAG-1-1912, 1(15):326-335*, 1994.
22. T. L. Brown. *The effect of long-term thermal cycling on the microcracking behavior and dimensional stability of composite materials.* PhD thesis, Virginia Polytechnic Institute and State University, 1997.
23. E. J. Barbero. *Introduction to Composite Materials Design, 3rd ed.* CRC Press, 2018.
24. E. J. Barbero. *Finite Element Analysis of Composite Materials Using Abaqus.* CRC Press, 2013.
25. A. Forghani, M. Shahbazi, N. Zobeiry, A. Poursartipand, and R. Vaziri. An overview of continuum damage models used to simulate intralaminar failure mechanisms in advanced composite materials. *Numerical Modelling of Failure in Advanced Composite Materials*, pages 151 – 173, 2015.
26. Adi Adumitroaie and E. J. Barbero. Intralaminar damage model for laminates subjected to membrane and flexural deformations. *Mechanics of Advanced Materials and Structures*, 22(9):705 – 716, 2015.
27. E. J. Barbero and J. Cabrera Barbero. Analytical solution for bending of laminated composites with matrix cracks. *Composite Structures*, 135:140 – 155, 2016.
28. Ever J Barbero and J. Cabrera Barbero. Determination of material properties for progressive damage analysis of carbon/epoxy laminates. *Mechanics of Advanced Materials and Structures, 26(11): 938-947*, 2019.
29. E. J. Barbero. *Finite Element Analysis of Composite Materials Using ANSYS.* CRC Press, 2014.
30. E. J. Barbero and D. C. Cortes. A mechanistic model for transverse damage initiation, evolution, and stiffness reduction in laminated composites. *Composites Part B, 41:124–132*, 2010.
31. M. M. Moure, S. Sanchez-Saez, E. Barbero, and E. J. Barbero. Analysis of damage localization in composite laminates using a discrete damage model. *Composites Part B: Engineering*, 66:224 – 232, 2014.
32. Mohammadhossein Ghayour, H. Hosseini-Toudeshky, M. Jalalvand, and E. J. Barbero. Micro/macro approach for prediction of matrix cracking evolution in laminated composites. *Journal of Composite Materials*, 50(19):2647–2659, 2016.
33. M. M. Moure, F. Otero, S. K. Garcia-Castillo, S. Sanchez-Saez, E. Barbero, and E. J. Barbero. Damage evolution in open-hole laminated composite plates subjected to in-plane loads. *Composite Structures*, 133:1048 – 1057, 2015.
34. M. M. Moure, S. K. Garcia-Castillo, S. Sanchez-Saez, E. Barbero, and E. J. Barbero. Influence of ply cluster thickness and location on matrix cracking evolution in open-hole composite laminates. *Composites Part B: Engineering*, 95:40 – 47, 2016.
35. D.S. Adams, D.E. Bowles, , and C.T. Herakovich. Characteristics of thermally-induced transverse cracks in graphite epoxy composite laminates. *NASA Technical Report TM-85429*, 1983.
36. R. G. Budinas and J. K. Nisbet. *Shigley's Mechanical Engineering Design, 10th ed.* McGraw Hill, 2015.
37. S. S. Sternstein. Yielding in glassy polymers. *Polymeric Materials, 369–410*, 1975.
38. H. H. Kausch. *Polymer Fracture, Polymers, Properties and Applications.* Springer Verlag, Berlin, 1978.
39. J. A. Nairn and S. Hu. *Damage Mechanics of Composite Materials*, chapter 6. Matrix Microcracking, pages 1–46. Elsevier, 1994.
40. E. J. Barbero. *Time-temperature superposition principle for predicting long-term response of linear viscoelastic materials*, chapter 2: Time-temperature-age superposition principle for predicting long-term response of linear viscoelastic materials, pages 48–69. Woodhead, Cambridge (ISBN978-1-84569-525-5), 2011.